Superconductivity in $Nb_{21}S_8$, a Phase with Metal Cluster Chains

Martin Köckerling,*,† Dirk Johrendt,‡ and E. Wolfgang Finckh§

Contribution from the Institut für Synthesechemie, Gerhard-Mercator-Universität, Lotharstrasse 1, D-47057 Duisburg, Germany, Institut für Anorganische Chemie und Strukturchemie der Heinrich-Heine-Universität, Universitätsstrasse 1, D-40225 Düsseldorf, Germany, and Institut für Anorganische Chemie und Analytische Chemie, Johannes-Gutenberg-Universität, Becherweg 24, D-55128 Mainz, Germany

Received June 15, 1998

Abstract: Phase pure samples of $Nb_{21}S_8$ are obtained by chemical transport and molten flux reactions in sealed niobium containers at 850−950 °C. In the temperature range from 5 to 290 K the electrical conductivity is found to be moderate metallic with a specific resistivity of 3.90 mΩ cm at 273 K. Magnetic susceptibility measurements give weak, almost temperature independent paramagnetism above ∼40 K. These metallic properties are compared with the structure of $Nb_{21}S_8$, which contains linear single and double chains of fused body centered niobium cubes, separated by S and additional Nb atoms. Both physical measurements consistently show a transition into the superconducting state below 4.1(5) and 3.7(2) K, respectively. Recently ideas were developed that superconductivity is favored by the tendency of pairwise attraction of conducting electrons at the Fermi level. To see whether these ideas can be applied to $Nb_{21}S_8$, electronic band structure calculations (TB-LMTO-ASA-method) have been performed. In fact at the X symmetry point the band structure shows two saddle points near the Fermi level giving rise to electron pairing. Other bands cut the Fermi level with large dispersion. These two band structure features are discussed as chemical requirements (fingerprints) for the occurrence of superconductivity in this three-dimensionally tightly bonded phase. Thereby, the applicability of this chemical picture of superconductivity is demonstrated on this system.

Introduction

During the past decade the outstanding superconducting properties of layered copper oxides have stimulated a great amount of scientific interest.[1] Intriguingly correlations between superconductivity and unique structural features are still not well developed. First steps in this direction are recent investigations which compare the bonding and electronic structure properties of layered copper oxides with those of layered rare-earth carbide halides of the type $RE_2X_2C_2^{2-6}$ (RE: rare earth element, X: halide) or of metal rich layered chalcogenides, like $Nb_xTa_{5-x}S_2$.[7] This last mentioned material belongs to an impressive array of new chemical compositions and structures which are found in the group of metal-rich chalcogenides of group 3 to 5.[8−14] One key feature of these compounds is a network of metal−metal bonds. Quite often parts of the metal atom arrangement resemble the structures of the elemental metals as for example bcc-metal units in $Nb_{21}S_8$,[15] Ta_2Se,[16] Nb_2Se,[17] or the "pseudo binary" $Nb_{0.40}Ta_{1.60}S$.[18,19] A different structural motif is found with interpenetrating metal icosahedra in dimorphic Ta_6S[20−22] (and isostructural substitution phases such as $M_xTa_{6-x}S$ (M = V, Cr)),[23] Ta_2S,[24] Ta_3S_2,[25−27] as well as in the tellurium-containing phases Ta_6Te_5[28] and $Ta_5(S,Te)_2$.[29] The structural similarities between the metal-rich chalcogenides and the elemental metals prompt a thorough investigation of the physical properties of the former, especially in the case of niobium

† Gerhard-Mercator-Universität Duisburg.
‡ Heinrich-Heine-Universität Düsseldorf.
§ Johannes-Gutenberg-Universität Mainz.

(1) Poole, C. P., Jr.; Farach, H. A.; Creswick, R. J. In *Superconductivity*; Academic Press: New York, 1995.
(2) Simon, A. *Angew. Chem.* **1997**, *109*, 1872.
(3) Bäcker, M.; Simon, A.; Kremer, R. K.; Mattausch, Hj.; Dronskowski, R.; Rouxel, J. *Angew. Chem.* **1996**, *108*, 837.
(4) Simon, A.; Yoshiasa, A.; Bäcker, M.; Henn, R. W.; Felser, C.; Kremer, R. K.; Mattausch, Hj. *Z. Anorg. Allg. Chem.* **1996**, *622*, 123.
(5) Simon, A.; Mattausch, Hj.; Eger, R.; Kremer, R. K. *Angew. Chem.* **1991**, *103*, 1210.
(6) Simon, A. *Angew. Chem.* **1987**, *99*, 602.
(7) Wang, Z.; Johnston, D. C.; Yao, X.; Franzen H. F. *Physica C* **1995**, 138.
(8) Franzen, H. F.; Köckerling, M. *Prog. Solid State Chem.* **1995**, *23*, 265.
(9) Franzen, H. F. *Prog. Solid State Chem.* **1978**, *12*, 1.
(10) Yao, X.; Marking, G.; Franzen, H. F. *Ber. Bunsen-Ges. Phys. Chem.* **1992**, *96*, 1552.
(11) Degen, T.; Harbrecht, B. *Angew. Chem.* **1995**, *107*, 2888.
(12) Degen, T.; Harbrecht, B. *Angew. Chem.* **1995**, *107*, 1226.
(13) Hughbanks, T. *J. Alloys Compd.* **1995**, *229*, 40.
(14) Neuhausen, J.; Finckh, E. W.; Tremel, W. *Inorg. Chem.* **1995**, *34*, 3823.
(15) Franzen, H. F.; Beinecke, T. A.; Conard, B. R. *Acta Crystallogr.* **1968**, *B24*, 412.
(16) Harbrecht, B. *Angew. Chem.* **1989**, *101*, 1696.
(17) Conard, B. R.; Norrby, L. J.; Franzen, H. F. *Acta Crystallogr.* **1969**, *B25*, 1729.
(18) Yao, X.; Miller, G. J.; Franzen, H. F. *J. Alloys Compd.* **1992**, *183*, 7.
(19) Nanjundaswamy, K. S.; Hughbanks, T. *J. Solid State Chem.* **1992**, *98*, 278.
(20) Franzen, H. F.; Smeggil, J. G. *Acta Crystallogr.* **1970**, *B26*, 125.
(21) Harbrecht, B. *J. Less-Common Met.* **1988**, *138*, 225.
(22) Nozaki, H.; Wada, H.; Takekawa, S. *J. Phys. Soc. Jpn.* **1991**, *60*, 3510.
(23) Harbrecht, B.; Franzen, H. F. *Z. Anorg. Allg. Chem.* **1987**, *551*, 74.
(24) Franzen, H. F.; Smeggil, J. G. *Acta Crystallogr.* **1969**, *B25*, 1736.
(25) Ahn, K.; Hughbanks, T. *J. Solid State Chem.* **1993**, *102*, 446.
(26) Kim, S. J.; Nanjundaswamy, K. S.; Hughbanks T. *Inorg. Chem.* **1991**, *30*, 159.
(27) Wada, H.; Onada M. *Mater. Res. Bull.* **1989**, *24*, 191.
(28) Conrad, M.; Harbrecht, B. *Euro. Conf. Solid State Chem., IVth*, **1992**, 324.
(29) Degen, T.; Harbrecht, B. *Angew. Chem.* **1995**, *107*, 2888.

10.1021/ja982081t CCC: $15.00
Published on Web 11/13/1998

Table 1. Experimental Details of the Reactions, Aiming for $Nb_{21}S_8$

no.	amount [mg]	loaded composition transport or flux material	T [°C]	time	side products (by Guinier)	lattice parameters a [Å]	lattice parameters c [Å]
1	100	$Nb_{21}S_8/NbCl_5$	950	34 d	~5% Nb	16.799(2)	3.3547(9)
2	100	$Nb_{21}S_8/Nb_3Cl_8$	950	34 d	~5% Nb	16.802(2)	3.356(1)
3	100	$Nb_{21}S_8/Nb_3I_8$	950	34 d	none	16.801(3)	3.354(1)
4	100	$Nb_{21}S_8$/CsCl	950	34 d	none (CsCl)	16.812(2)	3.3540(8)
5	300	$Nb_{21}S_8$/none	1400	1 hr	~10% NbS	16.807(3)	3.355(2)
6	700	$Nb_{21}S_8$/none	850	2 d	~5% Nb, ~5% NbS	16.820(2)	3.355(1)
7	200	$Nb_{21}S_{10}/NbCl_5$	950	14 d	none	16.809(4)	3.358(2)
8	200	$Nb_{21}S_{10}/NbCl_5$	950	21 d	none	16.813(2)	3.352(1)
9	200	$Nb_{21}S_{10}$	arc-melt./950	2 d	none	16.817(3)	3.357(1)

compounds, since elemental Nb is long known to be superconducting below 9.3 K.[30]

The phenomenon of (low temperature) superconductivity is observed in a rather large number of different compounds with many different structure types. But no trend that correlates a specific structure−property or stoichiometry feature with the value of T_c is recognizable. Within the chalcogenides two classes of compounds have attracted special interest: (1) Some hexagonal layered dichalcogenides 2H-MCh_2 (M: metal of group 4, 5, or 6; Ch: S, Se, Te) show superconductivity up to 7.0 K ($NbSe_2$) and exhibit pronounced anisotropy. Even higher T_c values (up to 13 K) are found in intercalated compounds.[31] (2) The Chevrel-phases MMo_6Ch_8, with M = Pb, Sn, La, Ag, ... (up to 40 elements), which contain octahedral metal-clusters which are face capped by Ch atoms and exhibit superconductivity up to 15 K even at high external magnetic fields.[32,33]

Here we report the synthesis of phase pure samples of $Nb_{21}S_8$, the structure of which has been published by Franzen et al.,[15] and results of magnetic susceptibility and electric resistivity measurements and discuss the observed properties with reference to the structure and theoretical expectations, derived from first principles electronic band structure calculations of the TB-LMTO type.

Experimental Section

General Techniques. The general synthetic techniques utilizing welded niobium ampules, as well as the Guinier-powder diffraction and cell parameter refinement methods, have been described elsewhere.[34,35] Unless otherwise noted all manipulations were carried out in nitrogen or argon filled dryboxes.

Synthesis. First hints of the possibility to synthesize $Nb_{21}S_8$ by chemical transport reactions or molten flux methods instead of the arc melting procedures which were used in the prior investigations[15] were obtained from reactions aiming for mixed niobium−halide−chalcogenide clusters (like Nb_6I_9S[36]). In the following reactions, aiming for phase pure samples of $Nb_{21}S_8$, a total of 100 to 700 mg of stoichiometric quantities of niobium powder (obtained from high purity Ames-Lab. Nb-sheets, as well as from Strem Chemicals, Inc., purity: 99.8%) and elemental sulfur (J. T. Baker and Aldrich, purity: 99.998%) together with less than 1 mg of halide transporting material ($NbCl_5$, $NbBr_5$, or NbI_5, sublimed prior to use) or about 100 mg of alkaline halide (CsCl as flux) were sealed in Nb ampules which in turn were encapsulated in silica jackets. All reactions were first heated at 450 °C for 2 days to allow for all the sulfur to react and then at 850−1400 °C for up to 34 days. One sample (no. 9, Table 1) was obtained by arc-melting of an appropriate mixture of NbS and Nb, followed by equilibration with $NbCl_5$, used as transporting agent, at 950 °C in a Nb ampule. To check the stability of $Nb_{21}S_8$ (especially with respect to the measurements of the superconducting state) against decomposition the powder pattern (see below) of one sample was retaken after exposure to air for 4 weeks. Both the line distribution and lattice parameters did not change significantly, confirming a stable phase. Experimental details for all reactions are given in Table 1.

Characterization. The phases obtained were identified by comparison of their Guinier powder patterns with those calculated on the basis of single-crystal data of known structures. The patterns were recorded with the microcrystalline samples held between two pieces of tape with the aid of Cu Kα radiation ($\lambda = 1.540562$ Å) on an Enraf-Nonius FR552 evacuable camera. The line positions, calibrated with the lines from Si as an internal standard, were used in least-squares routines to obtain precise lattice constants. Phase yields were estimated visually according to the relative intensity distribution on the Guinier films (with a detection limit of better than 5%).

Electric Resistivity Measurements. A microcrystalline sample of phase pure $Nb_{21}S_8$ was cold-pressed to a 0.6 mm thick layer onto a square array with 4 platinum electric contacts. The resistivity was measured as a function of temperature in the range from 290 to 3 K and in reverse at increments of 0.5−2 K with use of a current of 5 mA. Further measurements were performed on a larger chunk of material as well as on a single crystal with 2 contacts soldered with indium.

Magnetic Susceptibility Measurements. Magnetic susceptibility data were obtained on several samples of $Nb_{21}S_8$. The sample powders were held between two fused silica rods that were in turn fixed inside a silica tube, filled with He, and sealed at both ends. The measurements for the normal state properties were carried out at three temperatures between 40 and 306 K in 10 K steps with the aid of a Quantum Design MPMS SQUID magnetometer. Superconducting state data were measured with an external field H of 10 G between 2 and up to 20 K with the sample cooled with applied field (FC) as well as with zero field (ZFC). The data were corrected for the sample holder as well as for standard diamagnetic core contributions.[37]

To study the effect of increasing the external field strength on the magnetization, further measurements were performed with $H = 50$ G and $H = 100$ G.

Electronic Band Structure Calculations. To gain insight into the bonding of $Nb_{21}S_8$, especially with respect to superconductivity, the electronic band structure was calculated by using density functional theory with the local density approximation (LDA). The one-electron Schrödinger equation was solved self-consistently with the linear muffin-tin orbital (LMTO) method in the atomic-spheres-approximation (ASA) including the combined correction (CC).[38−40] This method splits the crystal space into overlapping atomic (Wigner−Seitz) spheres whose radii were chosen to fill the crystal volume completely. The one-electron potential entering the Schrödinger equation is a superposition

(30) Weast, R. C.; Astle, M. J.; Beyer, W. H., Eds. *CRC Handbook of Chemistry and Physics*, 65th ed.; CRC Press: Boca Raton, 1984.
(31) Wilson, J. A.; Di Salvo, F. J.; Mahajan, S. *Adv. Phys.* **1975**, *24*, 117.
(32) Foner, S.; Schwartz, B. B., Eds. *Superconductor Materials Science: Metallurgy, Fabrication and Applications*; Plenum Press: New York, 1981.
(33) Chevrel, R.; Hirrien, M.; Sergent, M. *Polyhedron* **1986**, *5*, 87.
(34) Köckerling, M.; Qi, R.-Y.; Corbett, J. D. *Inorg. Chem.* **1996**, *35*, 1437.
(35) Payne, M. W.; Corbett, J. D. *Inorg. Chem.* **1990**, *29*, 2246.
(36) Meyer, H.-J.; Corbett, J. D. *Inorg. Chem.* **1991**, *30*, 963.
(37) Selwood, P. W. *Magnetochemistry*; Interscience Publishers: New York, 1963; p 78.
(38) Andersen, O. K. *Phys. Rev.* **1975**, *B12*, 3060.
(39) Andersen, O. K.; Jepsen, O. *Phys. Rev. Lett.* **1984**, *53*, 2571.
(40) Jepsen, O.; Andersen, O. K. *Z. Phys.* **1995**, *B97*, 35.

Table 2. ASA Radii, Used in the TB-LMTO Calculations

atoms	ASA radii	atoms	ASA radii	atoms	ASA radii
Nb1	2.964	S2	2.583	E7	1.218
Nb2	3.012	E1	1.707	E8	1.102
Nb3	2.813	E2	1.633	E9	1.152
Nb4	2.801	E3	1.561	E10	1.034
Nb5	2.760	E4	1.440	E11	1.101
Nb6	2.934	E5	1.280	E12	1.040
S1	2.620	E6	1.321	E13	1.042

of overlapping spherical potential wells including a kinetic-energy error proportional to the relative overlap of the spheres. The ASA spheridizes the charge density inside the spheres and neglects the charge outside them. This would cause substantial errors due to large sphere overlap and misinterpretation of the potential. Therefore it is necessary to fill the void space with empty spheres. In general, the requirement for choosing the radii of atomic and empty spheres is that the superposition of the spherical potentials approximates the full three-dimensional potential as much as possible, that the overlap error is acceptable, and that the entire charge is inside the spheres, i.e., the sum of the spheres volumes (atomic plus empty spheres) must be equal to the unit cell volume.

The calculated atomic spheres radii and the radii of the added empty spheres (*E*), which were included to reduce the overlap of the atomic spheres below 16%, were calculated by using an automatic procedure developed by Krier et al.[42] and are given in Table 2. The atomic positions used are those from ref 15. All reciprocal space integrations were performed with the tetrahedron method,[41] using 14 irreducible k-points within the Brillouin zone. The muffin-tin orbitals included in the calculations were 5s, 5p, 4d, and 4f states for Nb and 3s, 3p, and 3d states for S. The 4f states of Nb and the 3d states of S were treated by the downfolding technique.[42]

Results and Discussion

Despite the enormous amount of effort that has been devoted to understand the fascinating property of superconductivity which is found in some complex layered copper oxides, this physical phenomenon is so far not understood when it comes to the correlation with structural parameters.[1] This is also true for the much longer known "conventional" superconductors, even though the general accepted theory from Bardeen, Cooper, and Shriffer (BCS theory) phenomenologically describes properties related by the superconducting state assuming a special form of electron pairing initiated by electron−phonon coupling (cooper pairs).[1]

Synthesis and Phase Distribution. To measure properties (and especially the superconductivity) of $Nb_{21}S_8$, phase pure samples were synthesized by chemical transport or molten flux methods. The samples obtained usually consisted of batches of thin needles, grown along [001], which were up to 2 mm long. Details of reaction conditions, products, and obtained lattice parameters are listed in Table 1.

Samples 1 and 2 contain besides $Nb_{21}S_8$ traces of elemental niobium. Since Nb is not found in reactions 7 and 8 which were run under similar conditions the first two were obviously a little niobium rich (sulfur deficient), possibly due to reaction of some sulfur with the Nb walls of the ampules in the early stages of the reaction. Loading slightly sulfur rich (nominal composition $Nb_{21}S_{10}$) takes care of this problem. Interestingly, no NbS_2, which can be chemically transported quite well,[43] is found in any reaction product. Only when reaction times are short, or if there is no transporting agent, and/or the reaction conditions are similar to the original annealing conditions following arc-melting,[15] is the binary NbS found as a side product.

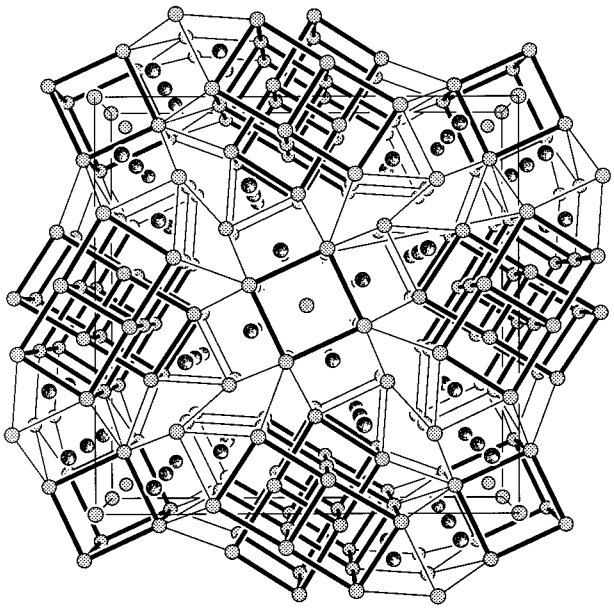

Figure 1. [001] view of the crystal structure of $Nb_{21}S_8$. Nb atoms are represented as regular dotted spheres, S atoms as irregular dotted spheres. The body centered cubic Nb units are emphasized.

The lattice parameters of the tetragonal cell, as obtained from least-squares refinement using the positions of the lines on the Guinier films, are also given in Table 1. They do not indicate any significant change in lattice parameters on changing the transporting agent. All values fall within a 4σ range of the average, $a = 18.809(3)$ Å and $c = 3.355(1)$ Å, values which are also close to the originally reported lattice parameters of $a = 16.794(5)$ Å and $c = 3.359(2)$ Å.[15] Furthermore, EDX measurements on a sample of reaction no. 8 (Table 1) do not give any indication of chloride incorporation into this sample.

Structural Features. Even though the structure of $Nb_{21}S_8$ has been described elsewhere,[15] we will discuss here those structural features which are important with respect to the observed properties. The most important structural feature of $Nb_{21}S_8$ is an extended network of metal−metal bonds. As depicted in Figure 1, two types of cluster chains, composed of body-centered Nb cubes as the smallest building blocks, run along [001] in the tetragonal structure.

The first cluster chain type is made of body-centered Nb cubes running along c which are condensed via opposing faces. The smallest unit of the second type of cluster chains consists of two face sharing body-centered Nb cubes. A second double-cube chain is fused into this, being rotated by 90° relative to the first one. Thereby the Nb atoms in the centers of the first double-cube chain are the edges of the shared face of the second double chain. These two types of "metal-tubing" as highlighted in Figure 1 show the close relation of this binary sulfide to the elemental niobium. In fact the Nb−Nb distances inside the cubes (2.82−2.95 Å) are as short as the shortest metal−metal distances in the elemental Nb (2.864 Å). In the compound the coordination environment is not perfectly cubic with edge lengths ranging from 3.202 to 3.427 Å. The metal-tube description of $Nb_{21}S_8$ shows some similarity to the β-tungsten structure of the Nb_3Z compounds (Z = Sn, Ga, Ge). These compounds are technologically used superconductors with T_c's above 18 K. The Nb atoms are arranged in Z-centered chains parallel to the edges of the cubic cell. They can be derived

(41) Jepsen, O.; Andersen, O. K. *Solid State Commun.* **1971**, *9*, 1763.
(42) Krier, G.; Jepsen, O.; Andersen, O. K. Unpublished results.
(43) Schäfer, H.; Fuhr, W. *J. Less-Common Met.* **1965**, *8*, 375.

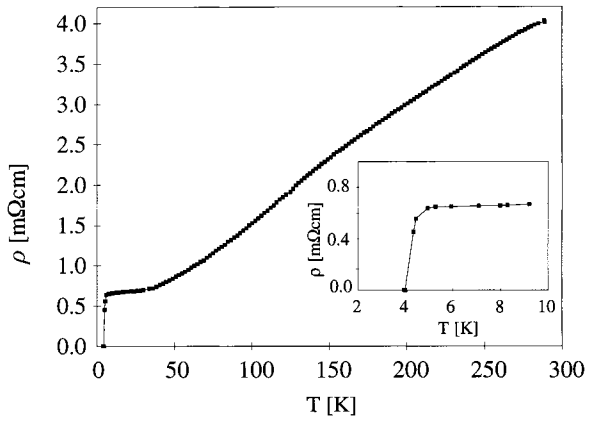

Figure 2. Temperature dependence of the specific resistivity of a microcrystalline sample of $Nb_{21}S_8$. The inset gives an enlarged view of the superconducting transition.

from Nb cubes, with the shared faces being distorted to rectangular (instead of square) planes.[44]

Using a different approach, the metal atom arrangement in $Nb_{21}S_8$ can be described as being built up from compressed and fused Nb_6 octahedra, allowing nicely for comparison with the structures of many other metal-rich compounds.[45] Further, recently investigated compounds which have interesting structural similarities to $Nb_{21}S_8$ are the isostructural $Zr_9Co_2P_4$ and $Zr_9Ni_2P_4$.[46]

Resistivity Measurements. From the extended metal−metal bonding, $Nb_{21}S_8$ can be expected to be a metallic conductor. Indeed, the results of the four-probe resistivity measurement of the cold pressed microcrystalline sample indicate metallic behavior in the temperature range from 5 to 290 K (Figure 2). The specific resistivity ρ at 273 K is 3.90 mΩ cm and decreases on lowering the temperature to 0.65 mΩ cm at 5 K. Comparable results were obtained from the two-point measurement on the larger chunk of sample as well as on a single crystal. Since the first mentioned measurement was performed on microcrystalline samples, where grain boundary effects and crystal defects cannot be estimated correctly, a direct comparison with the specific resistivity of the elemental niobium ($\rho_{(273)} = 12.5\ \mu\Omega$ cm[30]) is difficult. However, $Nb_{21}S_8$ with a much larger resistivity than that of elemental Nb is a moderate conductor. Similar resistivities are found for $Nb_{1.72}Ta_{3.28}S_2$.[7] This behavior is not completely unexpected from the structure, which can be understood as a metal diluted and ripped apart by sulfur atoms (see structural discussion above). At 4.1(5) K a major drop in resistivity occurs, indicating a transition into the superconducting state (Figure 2, inset).

Magnetic Measurements. The normal state metallic property, as found by the electric resistivity measurements, is confirmed by the results of magnetic measurements on sample no. 3 (Table 1) which are depicted in Figure 3. Above 40 K the magnetic susceptibility of $Nb_{21}S_8$ is paramagnetic in character and relatively small at room temperature in accordance with the metallic behavior found in the resistivity measurements. The superconducting transition occurs at $T_c = 3.7(2)$ K and is confirmed by the Meissner and diamagnetic shielding effect. Figure 4 shows the results of the measurements on sample no. 9. The same value of T_c is found for all the other samples (nos. 3, 4, 7, and 8).

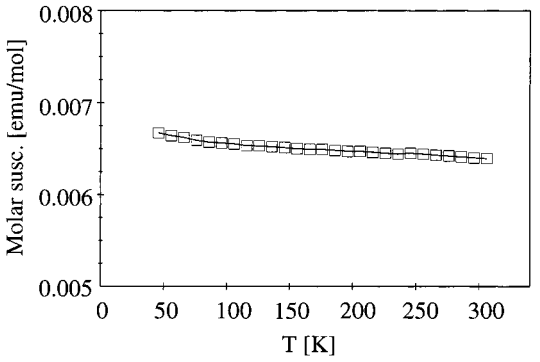

Figure 3. Temperature dependence of the molar magnetic susceptibility of a microcrystalline sample of $Nb_{21}S_8$ in the range of 40 to 306 K.

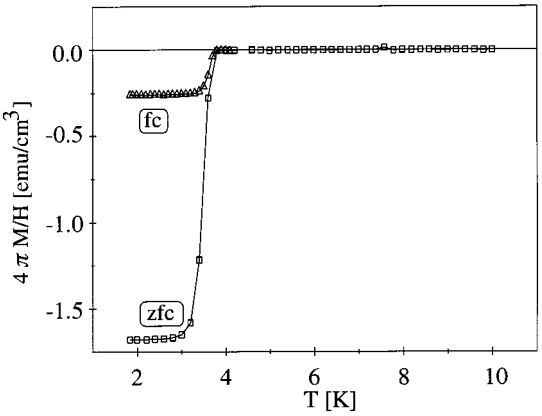

Figure 4. Transition into the superconducting state of $Nb_{21}S_8$ as shown by the diamagnetic shielding effect (zero field cooled data, zfc) and the Meissner effect (fc) using an external field of 10 G.

The superconducting transition occurs at $T_c = 3.7(2)$ K and is confirmed by the Meissner and the diamagnetic shielding effect (Figure 4). The width of the transition is 0.7 K. These samples do not show any indication of the occurrence of elemental niobium by an additional transition in the range of 9.0−9.5 K in the magnetization curves. That traces of niobium can be found in this way has been confirmed by the addition of Nb to a $Nb_{21}S_8$ sample. At this point it is of crucial importance to verify that $Nb_{21}S_8$ actually exhibits superconductivity and not some tiny amount of impurity like Nb oxides, NbS_2, or elemental Nb.[47] Therefore, the volume susceptibility $\chi_v = M\rho_x/H$, using the mass density $\rho_x = 7.739$ g/cm^3 as computed from the X-ray data,[15] was calculated. The value of $\chi_v = 0.021$ at 2.2 K (FC data), which is 26% of the theoretical value ($-1/4\pi$), indicates bulk superconductivity. Figure 5 shows zero-field-cooled magnetic data for three different field strengths. With increasing fields the transition broadens, the superconducting volume fraction decreases slightly, and the onset occurs at a slightly lower temperature (though this becomes more difficult to define as the transition broadens). These properties are consistent with a type II superconductor.[54]

(44) Hyde, B. G.; Andersson, S. *Inorganic Crystal Structures*; J. Wiley & Sons: New York, 1989; p 356ff.
(45) Simon, A. *Angew. Chem.* **1988**, *100*, 164.
(46) Kleinke, H.; Franzen, H. F. *Inorg. Chem.* **1996**, *35*, 5272.
(47) Buckel, W. *Supraleitung*; VCH Publishers: Weinheim, 1994.
(48) Bäcker, M.; Simon, A.; Kremer, R. K.; Mattausch, H.-J.; Dronskowski, R.; Rouxel, J. *Angew. Chem.* **1996**, *108*, 837.
(49) Simon, A. *Angew. Chem.* **1987**, *99*, 602.
(50) Simon, A.; Mattausch, H.-J.; Eger, R.; Kremer, R. K. *Angew. Chem.* **1991**, *103*, 1210.
(51) Mattausch, H.-J.; Simon, A.; Felser, C.; Dronskowski, R. *Angew. Chem.* **1996**, *108*, 1805.
(52) Simon, A.; Yoshiasa, A.; Bäcker, M.; Henn, R. W.; Felser, C.; Kremer, R. K.; Mattausch, Hj. *Z. Anorg. Allg. Chem.* **1996**, *622*, 123.
(53) Felser, C.; Cramm, S.; Johrendt, D.; Mewis, A.; Jepsen, O.; Hohlneicher, G.; Eberhardt, W.; Andersen, O. K. *Euro. Phys. Lett.* **1997**, *40*, 85.

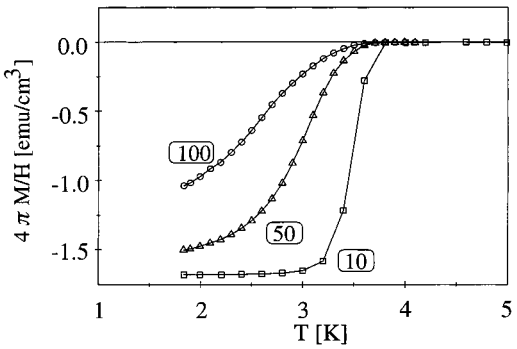

Figure 5. Zero field cooled magnetization data of the superconducting transition of $Nb_{21}S_8$ at external magnetic fields of 10, 50, and 100 G.

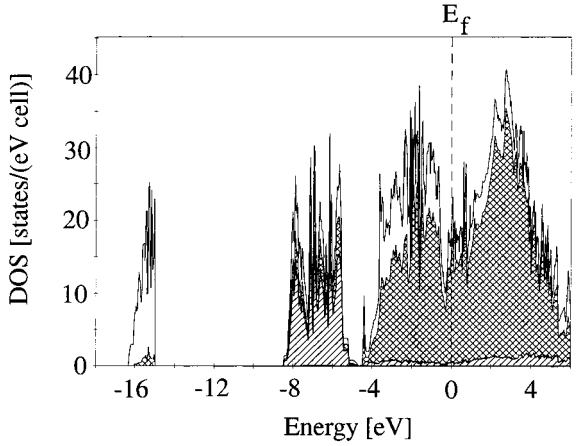

Figure 6. The total density of states (DOS) of $Nb_{21}S_8$ as obtained by self-consistent (LMTO) band structure calculations. The projection of all the sulfur p-functions is presented hatched and that of all the Nb d-functions is crosshatched. The dotted line marks the Fermi level E_F.

Electronic Band Structure Calculations. Electronic band structure calculations on $Nb_{21}S_8$ were performed with use of the TB-LMTO-ASA method.[38−40] The total density of states (DOS) together with the projection of sulfur p- and niobium d-levels is shown in Figure 6. The energy zero is taken at the Fermi level E_F. In the lower part the sulfur s-levels are located (from ca. −16.3 to −15 eV), which are clearly separated from the other states. The energy region from ca. −8.4 to −4.6 eV covers the sulfur p-functions. The Nb d-states are primarily located above these. The Fermi energy cuts through a maximum in the DOS curve with $N(E_F) = 20$ states/(eV cell). To analyze the bonding properties of the sulfur atoms a three-dimensional charge density grid was calculated. The S atoms appear as almost regular spheres indicating that it is possible to characterize them as S^{2-} ions. With the density of states at the Fermi level being composed of roughly 76% Nb d-states, it is clearly dominated by niobium states.

A small energy window of the LMTO-band structure in the vicinity of the Fermi level, calculated along several lines of high symmetry within the Brillouin zone, is depicted in Figure 7. The band structure is plotted from the zone border Z (0, $b^*/2$, 0) to the zone center Γ (0, 0, 0), and further to X ($a^*/2$, $b^*/2$, 0), P ($a^*/2$, $b^*/2$, $c^*/2$), and N (0, $b^*/4$, $c^*/2$). A graphical representation of this Brillouin zone showing the special symmetry points is given in Figure 9. Several high dispersive bands cut the Fermi level in accordance with the metallic properties. Also visible are bands (along Γ → X and X → P) which are basically flat in the vicinity of the Fermi level. These bands are responsible for the relatively high density of states at E_F. According to recent investigations of Simon et al., the occurrence of both types of bands can serve as a hint for the occurrence of superconductivity (fingerprint).[48−52] This hypothesis states that the tendency of the formation of superconducting Cooper pairs is favored by a pairwise localization of conduction electrons. Therefore flat bands which represent electronic states with small Fermi speed of the electrons as well as highly dispersive bands are necessary, i.e., the coexistence of localized electron pairs and itinerant electrons seems to be a

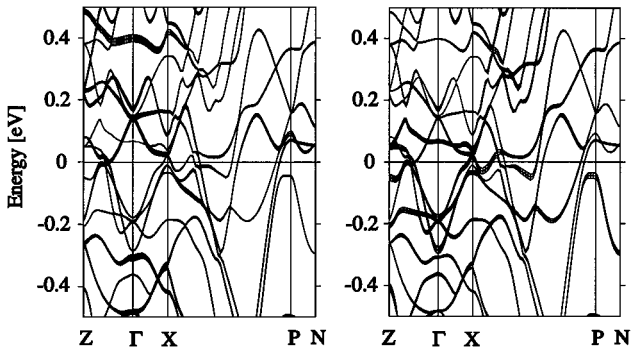

Figure 7. Fat-band representation of the Nb2 d-levels (left) and Nb6 d-levels (right) in the self-consistent band structure of $Nb_{21}S_8$ in the vicinity of the Fermi level.

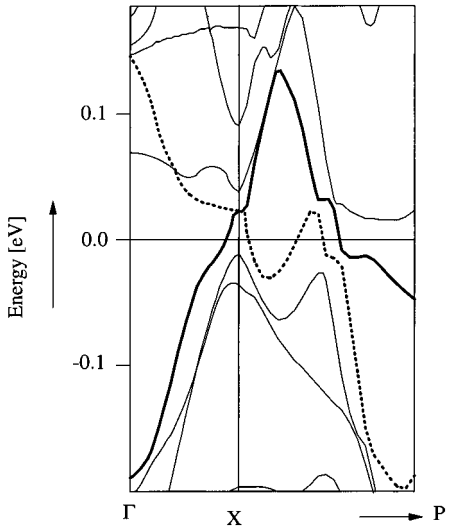

Figure 8. Expanded part of the band structure of $Nb_{21}S_8$ in the vicinity of the X-symmetry point at the Fermi level.

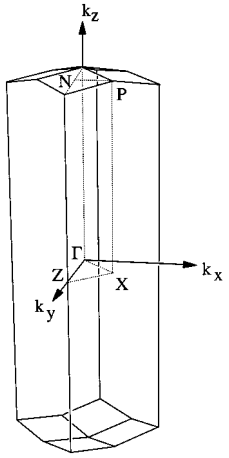

Figure 9. Plot of the Brillouin zone of $Nb_{21}S_8$ with the symmetry lines and points marked as used for the band structure calculations.

(54) Nagata, S.; Aochi, T.; Abe, T.; Ebisu, S.; Hagino, T.; Seki, Y.; Tsutsumi, K. *J. Phys. Chem. Solids* **1992**, *53*, 1259.

(chemically) necessary requirement for the occurrence of superconductivity. These features are observed in the band structures of layered oxocuprate superconductors as well as in the layered $(RE)_2X_2C_2$ (RE = Y, La; X = Cl, Br, I) and others.[2] At the X-symmetry point of the band structure of $Nb_{21}S_8$ two flat bands form a saddle point in the energy surface, coinciding almost with E_F (+0.02 eV). These so-called "van-Hove singularities" are discussed in attempts to explain the high-temperature superconductivity of some layered oxocuprates.[45−47,48,53] Figure 8 shows an expanded part of the band structure around the Fermi level at the X-symmetry point emphasizing these "van-Hove singularities". From the *fat band* representation which gives the orbital character proportional to the line widths it becomes clear that these bands are basically composed of Nb6-d and Nb2-d orbitals. The Nb2 and Nb6 atoms build up the cubic metal units in the crystal structure of $Nb_{21}S_8$. A more detailed analysis shows that antibonding Nb6-$d_{x^2-y^2}$ contributions form the band of the lower saddle point, whereas the higher one contains largely Nb6-d_{xz} + Nb6-d_{yz} + Nb2-d_{xz} + Nb2-d_{yz} states. This result shows that the observed superconductivity of $Nb_{21}S_8$ is in accordance with the recently developed ideas of the electronic requirements for superconductivity. Within the numerous investigations concerned with the phenomenon of superconductivity this work extends the chemical point of view which was developed on the basis of layered compounds toward the three-dimensionally tightly bonded system $Nb_{21}S_8$.

Acknowledgment. This work was supported by the Deutsche Forschungsgemeinschaft (DFG) through a postdoctoral fellowship (M.K.) and by the National Science Foundation, Solid State Chemistry (DMR-9510278). We thank J. D. Corbett, H. F. Franzen (Iowa State University, Ames, Iowa) for support and helpful discussions, J. Ostensen, P. Canfield, and I. Fisher (Iowa State University, Ames, Iowa) for the magnetic data, and G. Henkel (University of Duisburg, Germany), A. Mewis (University of Düsseldorf, Germany), and W. Tremel (University of Mainz, Germany) for their support. Thanks are also expressed to M. Barros (NPC GmbH, Düsseldorf, Germany) for a generous gift of niobium.

JA982081T